Solutions of mixed quantum-classical dynamics in multiple dimensions using classical trajectories

Chun-Cheng Wan and Jeremy Schofield[a)]
Chemical Physics Theory Group, Department of Chemistry, University of Toronto, Toronto, Ontario, M5S 3H6 Canada

(Received 9 August 2001; accepted 17 October 2001)

The multithreads algorithm for solving the mixed quantum-classical Liouville equation is extended to systems in which multiple classical degrees of freedom couple explicitly to a quantum subsystem. The method involves evolving a discrete set of matrices representing operators positioned at classical phase space coordinates according to precise dynamical rules dictated by evolution equations. The propagation scheme is based on the Trotter expansion of the time evolution operator and involves trajectory (thread) branching and pruning operations at each time step. The method is tested against exact numerical solution of the quantum dynamics for two models in which the nonadiabatic evolution of two heavy coordinates (nuclei) induces changes in population in two electronic states. It is demonstrated that the multithreads algorithm provides a good quantitative as well as qualitative description of the dynamics for branching ratios and populations as a function of time. Critical performance issues such as the computational demand of the method, energy conservation, and how the scheme scales with the number of classical degrees of freedom coupled to the quantum subsystem are discussed. © *2002 American Institute of Physics.*
[DOI: 10.1063/1.1425835]

I. INTRODUCTION

The idea of using classical trajectories to represent the time evolution of a large system in which quantum effects, such as tunneling, interference, and level quantization, influence the dynamics has been pursued by many authors.[1–12] There are two fundamentally different approaches to utilizing classical evolution schemes to describe the dynamics of a system exhibiting important quantum effects. The first is based upon semiclassical methods,[13] such as the initial value representation[8,14] method and its variants.[15] In the semiclassical approach, all degrees of freedom are treated on equal footing and trajectories evolve on the full classical phase space. Unfortunately, while these methods are very promising, the approximations that must be made in many semiclassical theories in order to obtain tractable expressions for observables are subtle and difficult to control. A quite different approach of representing the time evolution of quasiclassical systems is to concoct rules for combining a classical description of most of the degrees of the system while retaining a minimal level of quantum description for the remainder of the system. These methods are based on either *ad hoc* prescriptions for the way in which the classical and quantum systems interact and evolve,[4,5] on approximations applied to path integral propagators,[6,7] or on a mixed quantum-classical Liouville equation for a partially Wigner-transformed density matrix.[1,11,12,16–18]

In previous articles,[11,12] an algorithm of solving the mixed quantum-classical Liouville equation, termed the *multithreads method*, was proposed. The method relies on a finite representation of the partially Wigner-transformed density matrix in terms of matrices (or ''threads'') residing at points in the phase space of the classical subsystem. Similar ideas have appeared in the literature in the context of Liouville dynamics or wave-packet interferometry[18] as well in sophisticated methods for placing basis sets to solve the full Schrödinger equation.[19] The multithreads algorithm has been tested and demonstrated to provide an excellent description of the dynamics for models of proton transfer reactions[11,20] and scattering processes where interference effects are important.[4,12]

In this article, the multithreads algorithm is extended and tested on two simple two-dimensional models for which the full quantum solution is readily attainable. The importance of testing methods designed to model multidimensional nonadiabatic dynamics has been noted previously.[19] There are significant qualitative differences that can be observed in the quantum dynamics of one-dimensional versus higher-dimensional systems as true intersections between potential energy surfaces become possible in higher dimensions. In addition, in higher dimensions it is possible to circumvent regions on a given potential energy surface where nonadiabatic coupling to other surfaces is strong, and the topological structure of the energy surfaces can give rise to rich quantum features such as Berry's geometrical phase.[21,22] In Sec. II, the theoretical framework for describing the dynamics of mixed quantum-classical systems is reviewed and the importance of force operators acting on the classical degrees of freedom is stressed. In Sec. III, the ideas and assumptions underlying utilizing discrete representations for observables and propagating dynamical trajectories for the mixed quantum-classical systems is elaborated. In addition, the multithreads scheme, based upon an approximate effective time propagator constructed out of the full time evolution operator for the

[a)]Electronic mail: jmschofi@chem.utoronto.ca

mixed quantum-classical system, is outlined and issues pertaining to the scaling properties of the method with system size and convergence of the algorithm are discussed. In Sec. IV, the application of the method to model two multidimensional systems is presented and it is demonstrated that the multithreads approach gives good qualitative and quantitative results compared with those obtained from the numerical solution of the full quantum dynamics. Each of the models probes a different aspect of the multithreads method and together they form a comprehensive and challenging test of the multithreads technique. The first model considered in Sec. IV, the collinear reactive collision model, was originally devised by Ben-Nun and Martínez[23] to create a rigorous test of nonadiabatic methods for realistic physical systems. Although this model avoids harmonic and separable potentials, the simple form of the coupling of the diabatic surfaces precludes a thorough analysis of the scaling behavior of the multithreads algorithm. To examine the critical issue of how the method scales with the size of the system, a model of a conical intersection on a two-dimensional surface[24] is considered in which the functional dependence of the diabatic coupling matrix element on the spatial coordinates is complicated. For the conical intersection model, it is demonstrated that the multithreads algorithm can be implemented in a fashion in which the computational load scales linearly with the number of force commutation classes, which, at worst, also increases linearly with the dimension of the system. Furthermore, the method reproduces the time profile of important observables such as the branching probabilities very well over a wide range of coupling strengths, and is even capable of qualitatively reproducing more sensitive quantum features of the dynamics in the vicinity of the conical intersection.

II. THE EVOLUTION OF MIXED QUANTUM-CLASSICAL SYSTEMS

The mixed quantum-classical Liouville equation[1,11,16–18] provides a convenient framework for examining the evolution of a system in which a (usually) large subset $\hat{\mathbf{Q}}=(\hat{Q}_1,\ldots,\hat{Q}_{3N})$ of operators of the total degrees of freedom is described ''classically'' while the remaining degrees of freedom $\hat{\mathbf{q}}=(\hat{q}_1,\ldots,\hat{q}_{3n})$ are treated quantum-mechanically. The equation can be derived[1] from a perturbation expansion of the partial-Wigner transform[25] of the quantum Liouville equation in powers of a small parameter related to the ratio of the classical and quantum thermal wavelengths. From the quantum Liouville equation, one obtains

$$\frac{\partial\hat{\rho}_w(\mathbf{R},\mathbf{P},t)}{\partial t}=-i\hat{\mathcal{L}}\hat{\rho}_w(\mathbf{R},\mathbf{P},t), \tag{1}$$

where the subscript w refers to the partial Wigner transform operation, which can be represented for an arbitrary operator $\hat{A}$ as

$$\hat{A}_w(\mathbf{R},\mathbf{P})=\frac{1}{(2\pi\hbar)^{3N/2}}\int d\mathbf{z}\, e^{i\mathbf{P}\cdot\mathbf{z}/\hbar}\left\langle \mathbf{R}-\frac{\mathbf{z}}{2}\middle|\hat{A}\middle|\mathbf{R}+\frac{\mathbf{z}}{2}\right\rangle. \tag{2}$$

Note that, in general, since the partial Wigner transform is not performed with respect to all degrees of freedom, the transformed quantities are operators in the quantum subsystem which depend on the classical coordinates $\mathbf{R}$ and $\mathbf{P}$. The Liouville (super) operator $i\hat{\mathcal{L}}$ in Eq. (1) can be written in the abstract form

$$i\hat{\mathcal{L}}=i\hat{\mathcal{L}}^Q+i\hat{\mathcal{L}}^{\mathbf{P}}+i\hat{\mathcal{L}}^{\mathbf{R}}, \tag{3}$$

where

$$i\mathcal{L}^Q A_w(\mathbf{R},\mathbf{P})=\frac{i}{\hbar}[\hat{V}_w(\mathbf{R}),A_w(\mathbf{R},\mathbf{P})], \tag{4}$$

$$i\mathcal{L}^R A_w(\mathbf{R},\mathbf{P})=\frac{\mathbf{P}}{M}\cdot\nabla_{\mathbf{R}}A_w(\mathbf{R},\mathbf{P}), \tag{5}$$

$$i\mathcal{L}^P A_w(\mathbf{R},\mathbf{P})=\frac{1}{2}(\nabla_{\mathbf{P}}A_w(\mathbf{R},\mathbf{P})\cdot\hat{\mathbf{F}}+\hat{\mathbf{F}}\cdot\nabla_{\mathbf{P}}A_w(\mathbf{R},\mathbf{P})), \tag{6}$$

where $\mathbf{F}(\mathbf{R})=-\nabla_{\mathbf{R}}\hat{V}_w(\mathbf{R})$ is the ''force'' operator and $\hat{V}_w(\mathbf{R})$ is the partial Wigner transform of the full interaction potential $\hat{V}(\hat{\mathbf{Q}},\hat{\mathbf{q}})$. In Eqs. (4)–(6), and below, the inner product $\mathbf{A}\cdot\mathbf{B}$ denotes $\Sigma_{i=1}^{N}\mathbf{A}_i\cdot\mathbf{B}_i$. Equation (1) can be solved formally to obtain

$$\hat{\rho}_w(\mathbf{R},\mathbf{P},t)=e^{-i\hat{\mathcal{L}}t}\hat{\rho}_w(\mathbf{R},\mathbf{P}). \tag{7}$$

In the partial Wigner transform representation, expectation values or thermal average of an operator can be written in terms of the partial Wigner transform $\hat{\rho}_w(\mathbf{R},\mathbf{P})$ of the full density matrix $\hat{\rho}$ as

$$\langle A(t)\rangle=\mathrm{Tr}\int d\mathbf{R}\,d\mathbf{P}\,\hat{\rho}_w(\mathbf{R},\mathbf{P},t)\,\hat{A}_w(\mathbf{R},\mathbf{P}), \tag{8}$$

where the Tr operator performs a sum over an arbitrary but complete set of quantum system states. Although the thermal averages or expectation value of an operator is invariant to the choice of quantum basis, the actual form of the evolution equations for matrix elements of $\hat{\rho}_w$ depends on the particular representation of the quantum operators of the subsystem. Several different basis sets are commonly used to represent the quantum degrees of freedom, including the diabatic or subsystem basis, which diagonalizes the Hamiltonian of the quantum subsystem, and the adiabatic basis, which diagonalizes the partial Wigner transform of the Hamiltonian operator $\hat{H}_w(\mathbf{R},\mathbf{P})$ at fixed classical coordinates $\mathbf{R}$ and $\mathbf{P}$. In addition, it is sometimes useful to represent the evolution of the mixed quantum-classical systems in a basis set which diagonalizes a particular force operator $-\nabla_{R_i}V_w(\mathbf{R},\hat{\mathbf{q}})$.[11,12] Note that in the adiabatic and ''force'' bases, the basis-set wave functions depend parametrically on the classical coordinates $\mathbf{R}$ due to the coupling between the quantum subsystem and the classical degrees of freedom.

The mixed quantum-classical evolution equation can be represented in an arbitrary time-independent basis which depends parametrically on the classical coordinates $\mathbf{R}$ as

$$\frac{\partial \hat{\rho}_w^{\alpha\beta}(\mathbf{R},\mathbf{P},t)}{\partial t} = -(i\mathcal{L}^Q_{\alpha\beta,\alpha'\beta'} + i\mathcal{L}^R_{\alpha\beta,\alpha'\beta'} + i\mathcal{L}^P_{\alpha\beta,\alpha'\beta'}) \times \hat{\rho}_w^{\alpha'\beta'}(\mathbf{R},\mathbf{P},t), \tag{9}$$

where

$$i\mathcal{L}^Q_{\alpha\beta,\alpha'\beta'} = \delta_{\beta\beta'}\left(\frac{i}{\hbar}\hat{V}_w^{\alpha\alpha'}(\mathbf{R}) + \frac{\mathbf{P}}{M}\cdot\hat{\mathbf{D}}^{\alpha\alpha'}\right) - \delta_{\alpha\alpha'}\left(\frac{i}{\hbar}\hat{V}_w^{\beta'\beta}(\mathbf{R}) + \frac{\mathbf{P}}{M}\cdot\hat{\mathbf{D}}^{\beta'\beta}\right), \tag{10}$$

$$i\mathcal{L}^R_{\alpha\beta,\alpha'\beta'} = \delta_{\alpha\alpha'}\delta_{\beta\beta'}\frac{\mathbf{P}}{M}\cdot\nabla_{\mathbf{R}}, \tag{11}$$

$$i\mathcal{L}^P_{\alpha\beta,\alpha'\beta'} = \tfrac{1}{2}(\hat{\mathbf{F}}^{\alpha\alpha'}\delta_{\beta\beta'} + \hat{\mathbf{F}}^{\beta'\beta}\delta_{\alpha\alpha'})\cdot\nabla_{\mathbf{P}}, \tag{12}$$

with $\mathbf{F}^{\alpha\beta}(\mathbf{R}) = -\langle\alpha|\nabla_{\mathbf{R}}\hat{V}_w(\mathbf{R})|\beta\rangle$. In Eq. (10), $\mathbf{D}^{\alpha\beta}(\mathbf{R}) = \langle\alpha|\nabla_{\mathbf{R}}|\beta\rangle$ is the nonadiabatic coupling matrix in the time-independent basis. Note that the diabatic basis set is independent of the classical coordinates $\mathbf{R}$ and $\mathbf{P}$, which implies that $\mathbf{D}$ is zero in the diabatic representation.

When written in a given basis set, Eq. (9) can be conveniently expressed using supermatrix notation in which all matrix elements $\rho_w^{\alpha\beta}$ are represented as elements of a single supervector ρ_w^{μ}, with μ representing the pair (α,β) as

$$\rho_w^{\mu}(t) = (e^{-i\mathcal{L}t})_{\mu\nu}\rho_w^{\nu}(0). \tag{13}$$

A number of methods of tackling the numerical solution of (13) are potentially feasible. One possibility is to separate the Liouville supermatrix operator $i\mathcal{L}$ into a classical coordinate propagation part $i\mathcal{L}^{cl} = i\mathcal{L}^R + i\mathcal{L}^P$ and a quantum rotation $i\mathcal{L}^Q$ component. Based on symmetries of the superoperator matrices, it can be shown that each component of the supermatrix operator has purely imaginary eigenvalues, so that the Trotter product formula[26]

$$e^{-i(\mathcal{L}^{cl}+\mathcal{L}^Q)t} = (e^{-i\mathcal{L}^{cl}t/2N_t}e^{(-i\mathcal{L}^Q t/N_t)}e^{(-i\mathcal{L}^{cl}t/2N_t)})^{N_t} + O(N^{-2}), \tag{14}$$

may be applied to approximate propagation over the total time interval as propagation over N_t short-time segments of duration Δt, with $t = N_t\Delta t$

$$\hat{\rho}_w(t) = e^{-i\mathcal{L}^{cl}\Delta t/2}M_q(\Delta t)\cdots M_q(\Delta t)e^{-i\mathcal{L}^{cl}\Delta t/2}\hat{\rho}_w(0), \tag{15}$$

with the quantum rotation matrix $M_q(\Delta t)$ given by

$$M_q^{\mu\nu}(\Delta t) = (e^{-i\mathcal{L}^Q\Delta t})_{\mu\nu}. \tag{16}$$

The Trotter formula may be applied once again to further decompose the operation of classical propagator part $i\mathcal{L}^{cl} = i\mathcal{L}^R + i\mathcal{L}^P$ into a velocity Verlet form[27]

$$e^{-i\mathcal{L}^{cl}\Delta t} \approx e^{-i\mathcal{L}^P\Delta t/2}e^{-i\mathcal{L}^R\Delta t}e^{-i\mathcal{L}^P\Delta t/2}. \tag{17}$$

For multidimensional systems, the Trotter formula must be applied once again if the force operators appearing in $i\mathcal{L}^P$ do not commute. For example, for a two-dimensional system in which the force operators $\hat{F}_1 = -\nabla_{R_1}\hat{V}_w(\mathbf{R})$ and $\hat{F}_2 = -\nabla_{R_2}\hat{V}_w(\mathbf{R})$ do not commute, the momentum propagator can be further decomposed as

$$e^{-i\mathcal{L}^P\Delta\tau} \approx e^{-i\mathcal{L}^{P_1}\Delta\tau/2}e^{-i\mathcal{L}^{P_2}\Delta\tau}e^{-i\mathcal{L}^{P_1}\Delta\tau/2}, \tag{18}$$

where

$$i\mathcal{L}^{P_i}\hat{A}_w(\mathbf{R},\mathbf{P}) = \tfrac{1}{2}(\nabla_{P_i}\hat{A}_w(\mathbf{R},\mathbf{P})\hat{F}_i + \hat{F}_i\nabla_{P_i}\hat{A}_w(\mathbf{R},\mathbf{P})). \tag{19}$$

In general, any function of only classical coordinates which are not explicitly coupled to the quantum subsystem is diagonal in the orthonormal representation of the quantum subsystem. All forces arising from such classical degrees of freedom therefore commute in the quantum representations and can be treated without further Trotter decomposition. These degrees of freedom evolve in an entirely classical fashion and are affected by the quantum subsystem only through their interactions with other classical degrees of freedom coupled directly to quantum subspace operators.

It is also possible to decompose the propagator in other ways. For example, in a two-dimensional system one may apply the Trotter decomposition along each dimension of the system by writing $i\mathcal{L}^{cl} = i\mathcal{L}^{cl_1} + i\mathcal{L}^{cl_2}$, and

$$e^{-i\mathcal{L}^{cl}\Delta t} \approx e^{-i\mathcal{L}^{cl_1}\Delta t/2}e^{-i\mathcal{L}^{cl_2}\Delta t}e^{-i\mathcal{L}^{cl_1}\Delta t/2}, \tag{20}$$

where $i\mathcal{L}^{cl_i} = i\mathcal{L}^{R_i} + i\mathcal{L}^{P_i}$. The propagation along each pair (R_i,P_i) of classical coordinates may then be separated into spatial and momentum propagation steps as in Eq. (17). Although there is no clear basis for the preference of one choice of decomposition of the propagator over another, the conventional choice of propagation scheme is to update all the spatial and momentum coordinates in a sequential fashion. In all the simulation results presented in Sec. IV, both schemes were utilized and little difference in performance of the multithreads algorithm was observed.

The evaluation of the action of the momentum propagator $\exp -i\mathcal{L}^{P_i}t$ on dynamical variables is complicated by the fact that the $i\mathcal{L}^{P_i}$ may not be diagonal in the reference basis used to represent the quantum subsystem. The effect of the momentum propagator on an arbitrary supermatrix element ν of a P_i-dependent operator $f^{\nu}(P_i)$ can be examined by introducing the unitary matrix $U_i(\mathbf{R})$ which diagonalizes the Liouville operator for the momenta

$$U_i^{-1}(\mathbf{R})i\mathcal{L}^{P_i}U_i(\mathbf{R}) = i\tilde{\mathcal{L}}_d^{P_i}. \tag{21}$$

By inspection of Eq. (6), it is evident that the unitary supermatrix which diagonalizes $i\mathcal{L}^{P_i}$ can be written as a Cartesian product of the unitary matrix which diagonalizes the force operator F_i represented in the reference basis. Using the identity $U^{-1}(\mathbf{R})U(\mathbf{R}) = \mathbf{I}$, where $\mathbf{I}$ is the unit supermatrix, one obtains

$$(e^{-i\mathcal{L}^{P_i}\Delta\tau})_{\mu\nu}f^{\nu}(P_i) = U_i^{\mu\gamma}(\mathbf{R})(e^{-i\tilde{\mathcal{L}}_d^{P_i}\Delta\tau})_{\gamma\gamma}\tilde{f}^{\gamma}(P_i) = U_i^{\mu\gamma}(\mathbf{R})\tilde{f}^{\gamma}(P_i - F_i^{\gamma}\Delta\tau), \tag{22}$$

where repeated indices are summed over, F_i^{γ} are the forces of the diagonalized operator, $i\tilde{\mathcal{L}}^{P_i}$, and $\tilde{f}^{\gamma}(P_i) = U_i^{-1\gamma\nu}(\mathbf{R})f^{\nu}(P_i)$. From Eq. (22) it is evident that the ac-

tion of the momentum propagator superoperator on a dynamical variable can be evaluated by transforming the dynamical variable into the representation in which the momentum propagator superoperator is diagonal and then propagating *each* matrix element of the transformed variable according to the force for this element. Note that the subsequent transformation of the dynamical variable back to the original representation mixes the phase space arguments since the momenta for each element may have evolved to different values. The mixing of phase space arguments for the matrix elements of dynamical variables complicates the interpretation of the evolution scheme based on the Trotter expansion. In the next section, however, we show that a discrete representation of dynamical operators (or the density matrix) offers a transparent structure for interpreting the evolution scheme in terms of branching trajectories.

III. DISCRETE REPRESENTATIONS OF OBSERVABLES AND APPROXIMATE SOLUTIONS OF MIXED QUANTUM-CLASSICAL DYNAMICS

Averages of dynamical variables over densities (typically probability densities) as expressed in Eq. (8) are commonly performed in analytically untractable systems by averaging a finite number of trajectories starting from initial coordinates selected to represent the density. The initial coordinates are generally taken as either weighted points on a grid for low-dimensional systems or as randomly drawn points with a probability determined by the density using Monte Carlo or other methods. In such cases, a time correlation function $\langle AB(t)\rangle$ can be approximated as

$$\begin{aligned}\langle AB(t)\rangle &= \int d\mathbf{R}\, d\mathbf{P}\rho(\mathbf{R},\mathbf{P})A(\mathbf{R},\mathbf{P})B(\mathbf{R}(t),\mathbf{P}(t))\\ &= \int d\mathbf{R}\, d\mathbf{P}[e^{-i\mathcal{L}t}(\rho(\mathbf{R},\mathbf{P})A(\mathbf{R},\mathbf{P}))]B(\mathbf{R},\mathbf{P})\\ &\approx \int d\mathbf{R}\, d\mathbf{P}\sum_{i=1}^{L}[e^{-i\mathcal{L}t}(W_i\delta(\mathbf{R}-\mathbf{R}_i)\\ &\quad\times\delta(\mathbf{P}-\mathbf{P}_i))]B(\mathbf{R},\mathbf{P}),\end{aligned} \tag{23}$$

where $i\mathcal{L}$ is the classical Liouville operator, W_i is the "weight" of the initial phase point $(\mathbf{R}_i,\mathbf{P}_i)$, and L is the number of initial points sampled from the density $\rho(\mathbf{R},\mathbf{P})A(\mathbf{R},\mathbf{P})$. The statistical properties of the average are typically monitored as a function of the initial points L which is increased until the desired level of statistical uncertainty is reached. Provided the density and the dynamical variable are smooth functions of their phase space arguments $\mathbf{R}$ and $\mathbf{P}$ at all times, L is generally found to be a relatively modest number (i.e., not prohibitively large) even for large systems. An implicit assumption in this approach is the existence of "shadow" orbits[28] in which trajectories generated by approximate numerical methods track true trajectories. Although this shadowing property has not been proven for any complicated dynamical systems, it is generally considered to hold for real systems.[29]

Based on the success of applying trajectory methods to problems in classical statistical mechanics, it is interesting to consider to what extent a trajectory approach based on finite representations of phase space integrals is useful in the context of mixed quantum-classical dynamics. To pursue this line, suppose that the partial Wigner transform of the arbitrary operator is represented by the finite phase space matrix density

$$\hat{B}_w(\mathbf{R},\mathbf{P}) = \sum_{j=1}^{L} \mathbf{W}_j\, \delta(\mathbf{R}-\mathbf{R}_j)\, \delta(\mathbf{P}-\mathbf{P}_j), \tag{24}$$

where $\mathbf{W}_j$ is a matrix representing the quantum character of the operator. The matrix $\mathbf{W}$ is weighted according to the phase space arguments for each point or "thread." Note that for a purely classical variable for which $\hat{B}_w(\mathbf{R},\mathbf{P}) = \mathbf{I}B(\mathbf{R},\mathbf{P})$, $\mathbf{W}=\mathbf{I}$. For an operator $g(\hat{\mathbf{q}})$ of the quantum subsystem alone, on the other hand, $\mathbf{W}_j$ is independent of the thread index j. The utility of the discretization approach depends on the accuracy of representing any observable of physical interest [or, equivalently, the transformed density matrix $\hat{\rho}_w(\mathbf{R},\mathbf{P},t)$] by a finite and manageable number of matrices located at discrete points in classical phase space.

In particular, looking at the partial Wigner transform of the density matrix, the solution we are seeking is the discretized form

$$\hat{\rho}^d(\mathbf{R},\mathbf{P},t) = \sum_{j=1}^{L} \hat{\theta}_j(t)\,\delta(\mathbf{R}-\mathbf{R}_j(t))\,\delta(\mathbf{P}-\mathbf{P}_j(t)), \tag{25}$$

where the $\hat{\theta}_j(t)$ are positive definite matrices. Equation (25) can be viewed as a summation over points or threads which compose the discrete representation of the density matrix. Note that the normalization condition implies

$$\mathrm{Tr}\int_{\Omega} d\mathbf{R}\, d\mathbf{P}\hat{\rho}^d(\mathbf{R},\mathbf{P},t) = \mathrm{Tr}\sum_j\, \hat{\theta}_j(t) = 1, \tag{26}$$

where Tr is the trace over the quantum subspace and the phase space integral is restricted to the regions of phase space where $\hat{\rho}_w$ is nonzero. The discretization should be useful under the following conditions:

(1) *At all times, the density matrix $\hat{\rho}(\mathbf{R},\mathbf{P},t)$ is confined to a finite volume Ω in the phase space, outside of which the magnitude of the density matrix elements becomes negligible.*

(2) *At all times, all physical operators $\hat{B}_w(\mathbf{R},\mathbf{P})$ (including $\hat{\rho}_w$ itself) are smooth functions of $\mathbf{R}$ and $\mathbf{P}$, with eigenvalues bounded from below.*

These conditions imply that there exists a finite number of threads L for an arbitrarily small but finite number $\epsilon>0$ such that

$$\left|\mathrm{Tr}\int_{\Omega} d\mathbf{R}\, d\mathbf{P}[\hat{\rho}_w(\mathbf{R},\mathbf{P},t)\hat{B}_w(\mathbf{R},\mathbf{P}) - \hat{\rho}^d(\mathbf{R},\mathbf{P},t)\hat{B}_w(\mathbf{R},\mathbf{P})]\right| < \epsilon, \tag{27}$$

where the time dependence of $\hat{\rho}_w(\mathbf{R},\mathbf{P},t)$ is determined by the mixed quantum-classical Liouville equation.

Now, suppose that initially at $t=0$, $\hat{\rho}^d(R,P,0)$ satisfies Eq. (27). Then, the following argument indicates that $\hat{\rho}^d(\mathbf{R},\mathbf{P},t)$, where

$$\hat{\rho}^d(\mathbf{R},\mathbf{P},t)=e^{-i\mathcal{L}t}\hat{\rho}^d(\mathbf{R},\mathbf{P},0), \tag{28}$$

also satisfies (27) at time t provided ϵ is sufficiently small. For the convenience of the argument, we consider instead of the delta functions the other bases to span the phase space, such as the fixed width Gaussian $g(R-R_i)$ and $g(P-P_i)$, which propagate under the classical propagator just "like" the delta function. The delta function can be approached in the limit that the width goes to zero. Under these circumstances, it follows that there exists a set of $\hat{\theta}_j$ with finite total number M, such that inequality (27) is satisfied, and $\hat{\rho}(\mathbf{R},\mathbf{P},0)-\hat{\rho}^d(\mathbf{R},\mathbf{P},0)\geqslant 0$. Furthermore, the fact that the eigenvalues of all operators have a lower bound implies that $\hat{B}_w(\mathbf{R},\mathbf{P})$ can be converted into a positive definite matrix by adding to it a trivial constant.

From these properties, it follows that

$$\begin{aligned}
&\left|\mathrm{Tr}\int_\Omega d\mathbf{R}\,d\mathbf{P}[\hat{\rho}_w(\mathbf{R},\mathbf{P},t)\hat{B}_w(\mathbf{R},\mathbf{P})-\hat{\rho}^d(\mathbf{R},\mathbf{P},t)\hat{B}_w(\mathbf{R},\mathbf{P})]\right| \\
&\quad=\left|\mathrm{Tr}\int_\Omega d\mathbf{R}\,d\mathbf{P}e^{-i\mathcal{L}t}[\hat{\rho}_w(\mathbf{R},\mathbf{P},0)\hat{B}_w(\mathbf{R},\mathbf{P})\right. \\
&\qquad\left.-\hat{\rho}^d(\mathbf{R},\mathbf{P},0)\hat{B}_w(\mathbf{R},\mathbf{P})]\right|. \\
&\quad\leqslant \mathrm{Tr}\int_\Omega d\mathbf{R}\,d\mathbf{P}[e^{-i\mathcal{L}t}]^2\times\mathrm{Tr}\int_\Omega d\mathbf{R}\,d\mathbf{P}[(\hat{\rho}_w(\mathbf{R},\mathbf{P},0) \\
&\qquad-\hat{\rho}^d(\mathbf{R},\mathbf{P},0))\hat{B}_w(\mathbf{R},\mathbf{P})]^2 \\
&\quad\leqslant d_q\Omega\left[\mathrm{Tr}\int_\Omega d\mathbf{R}\,d\mathbf{P}(\hat{\rho}_w(\mathbf{R},\mathbf{P},0)\right. \\
&\qquad\left.-\hat{\rho}^d(\mathbf{R},\mathbf{P},0))\hat{B}_w(\mathbf{R},\mathbf{P})\right]^2\leqslant d_q\Omega\epsilon^2,
\end{aligned} \tag{29}$$

where d_q is the dimension of the quantum subspace. To obtain the relation above, we have applied the generalized Cauchy–Schwartz inequality. From these considerations, it is evident that Eq. (27) is satisfied provided that $\epsilon d_q\Omega<1$. These results suggest that if the initial discrete representation of the partial Wigner-transformed density matrix is sufficiently accurate, dynamical evolution of the approximate density matrix preserves the quality of the discrete representation at subsequent times under conditions (1) and (2).

We now turn our attention to examining the nature of the action of the Trotter-factorized propagator on the discrete representation of an arbitrary dynamical variable expressed as in Eq. (24). In particular, we must evaluate how the following propagators act on the finite representations of the dynamical variable $B_w(\mathbf{R},\mathbf{P})$:

$$e^{-i\mathcal{L}^Q\delta t}B_w(\mathbf{R},\mathbf{P})=e^{-i\mathcal{L}^Q\delta t}\sum_{j=1}^{L}\mathbf{W}_j\delta(\mathbf{R}-\mathbf{R}_j)\,\delta(\mathbf{P}-\mathbf{P}_j), \tag{30}$$

$$e^{-i\mathcal{L}^R\delta t}B_w(\mathbf{R},\mathbf{P})=e^{-i\mathcal{L}^R\delta t}\sum_{j=1}^{L}\mathbf{W}_j\delta(\mathbf{R}-\mathbf{R}_j)\,\delta(\mathbf{P}-\mathbf{P}_j), \tag{31}$$

$$e^{-i\mathcal{L}^P\delta t}B_w(\mathbf{R},\mathbf{P})=e^{-i\mathcal{L}^P\delta t}\sum_{j=1}^{L}\mathbf{W}_j\delta(\mathbf{R}-\mathbf{R}_j)\,\delta(\mathbf{P}-\mathbf{P}_j), \tag{32}$$

where the $i\mathcal{L}^Q$, $i\mathcal{L}^R$, and $i\mathcal{L}^P$ are defined in Eq. (9). First, the operator $i\mathcal{L}^Q$ does not involve derivatives with respect to the classical coordinates and therefore operates only on the quantum subspace of the dynamical variable. In supervector notation, we therefore obtain

$$\begin{aligned}
&(e^{-i\mathcal{L}^Q\delta t})_{\mu\nu}\sum_{j=1}^{L}\mathbf{W}_j^\nu\delta(\mathbf{R}-\mathbf{R}_j)\,\delta(\mathbf{P}-\mathbf{P}_j) \\
&\quad=\sum_{j=1}^{L}\mathbf{W}_j^\mu(\delta t)\,\delta(\mathbf{R}-\mathbf{R}_j)\,\delta(\mathbf{P}-\mathbf{P}_j),
\end{aligned} \tag{33}$$

where $\mathbf{W}_j^\mu(\delta t)$ is easily evaluated by transforming to and from the basis in which the superoperator $i\mathcal{L}^Q$ is diagonal. Since the operator $i\mathcal{L}^R$ is diagonal in the quantum subspace, the evaluation of (31) is straightforward, yielding

$$\begin{aligned}
&e^{-i\mathcal{L}^R\delta t}\sum_{j=1}^{L}\mathbf{W}_j\delta(\mathbf{R}-\mathbf{R}_j)\,\delta(\mathbf{P}-\mathbf{P}_j) \\
&\quad=\sum_{j=1}^{L}\mathbf{W}_j\delta(\mathbf{P}-\mathbf{P}_j)e^{-i\mathcal{L}^R\delta t}\delta(\mathbf{R}-\mathbf{R}_j) \\
&\quad=\sum_{j=1}^{L}\mathbf{W}_j\delta(\mathbf{P}-\mathbf{P}_j)e^{i\mathcal{L}^R(\mathbf{R}_j,\mathbf{P}_j)\delta t}\delta(\mathbf{R}-\mathbf{R}_j) \\
&\quad=\sum_{j=1}^{L}\mathbf{W}_j\delta(\mathbf{R}-(\mathbf{R}_j+\delta tP_j/m))\,\delta(\mathbf{P}-\mathbf{P}_j),
\end{aligned} \tag{34}$$

where the spatial derivatives in $i\mathcal{L}^R(\mathbf{R}_j,\mathbf{P}_j)$ are with respect to the thread coordinate $\mathbf{R}_j$ and $\mathbf{P}$ has been replaced by $\mathbf{P}_j$.

The action of the momentum propagator $i\mathcal{L}^P$ on the dynamical variable is somewhat more complicated due to the off-diagonal forces. Using the transformation matrices introduced in Eq. (22), Eq. (32) can be written for the momentum propagator of a particular component P_k as

$$\begin{aligned}
&(e^{-i\mathcal{L}^{P_k}\delta t})_{\mu\nu}\sum_{j=1}^{L}\mathbf{W}_j^\nu\delta(\mathbf{R}-\mathbf{R}_j)\,\delta(\mathbf{P}-\mathbf{P}_j) \\
&\quad=\sum_{j=1}^{L}U_k^{\mu\gamma}(\mathbf{R})(e^{i\tilde{\mathcal{L}}_d^{P_k}\Delta\tau})_{\gamma\gamma}\tilde{\mathbf{W}}_j^\gamma\delta(\mathbf{R}-\mathbf{R}_j)\,\delta(\mathbf{P}-\mathbf{P}_j) \\
&\quad=\sum_{j=1}^{L}U_k^{\mu\gamma}(\mathbf{R})\tilde{\mathbf{W}}_j^{k,\gamma}\delta(\mathbf{R}-\mathbf{R}_j)\,\delta(\mathbf{P}-\mathbf{P}_j^{k,\gamma}(\delta t)),
\end{aligned}$$

where $\mathbf{P}_j^{k,\gamma}(\delta t)=(P_1,\ldots,P_{k-1},P_k+F_k^\gamma\delta t,\ldots,P_N)$ and $\tilde{\mathbf{W}}^k=U_k^{-1}(\mathbf{R})\cdot\mathbf{W}$. Again, note that, in general, each component $\tilde{W}^\gamma$ of the supervector $\tilde{\mathbf{W}}$ evolves according to a different force, F^γ. Suppose that the effective dimension of the quantum subspace is d_q so that the supervector $\tilde{\mathbf{W}}$ is a D-dimensional column vector, where $D=d_q*(d_q+1)/2$, which can be decomposed as follows:

$$\tilde{\mathbf{W}} = \begin{pmatrix} w_1 \\ w_2 \\ \vdots \\ w_D \end{pmatrix} = \begin{pmatrix} w_1 \\ 0 \\ \vdots \\ 0 \end{pmatrix} + \begin{pmatrix} 0 \\ w_2 \\ \vdots \\ 0 \end{pmatrix} + \cdots + \begin{pmatrix} 0 \\ 0 \\ \vdots \\ w_D \end{pmatrix}$$

$$= \tilde{\mathbf{X}}_1 + \tilde{\mathbf{X}}_2 + \cdots + \tilde{\mathbf{X}}_D . \tag{35}$$

The matrix product $U_k(\mathbf{R})\tilde{\mathbf{W}}^k$ in Eq. (35) implies that every thread may be written as a linear combination of D new threads with a supervector $U_k(\mathbf{R})\tilde{\mathbf{X}}_i$, where each of the threads has different P_k arguments. From these considerations, one may interpret the consequence of the off-diagonal nature of the momentum propagator as leading to the branching of one thread into D new threads along each of the $3N$ momentum degrees of freedom. Hence, the total number of threads after a *single* momentum propagation step along a particular degree of freedom increases by a factor of D from the current number L to $D\times L$. Clearly, the number of threads grows exponentially with propagation time step and with the number of noncommuting force matrices.

One can thus summarize the propagation scheme as follows: For each time step, the spatial coordinates are updated according to Eq. (35). After all spatial coordinates have been updated, the transformation supermatrices $U_k(\mathbf{R})$ are constructed and the momenta P_k are updated in sequential fashion. This is carried out by transforming the supervector $\mathbf{W}$ for each of the threads into the appropriate force representation in which the momentum propagator of P_k is diagonal. D threads are created from each old thread out of the individual elements of $\mathbf{W}$ and the momentum argument for the phase point for each of them is propagated with the diagonal forces for that element. After propagation, all threads are transformed back into the original representation and the process is repeated. Following the propagation of all momenta, the supervectors undergo a quantum rotation as described in Eq. (33).

On the other hand, according to the arguments concerning Eq. (27), only L threads should be sufficient to describe to represent the dynamical variable accurately (to order ϵ). Hence, from a practical point of view, since the function the threads represent is localized in finite regions of phase space and relatively smooth by assumption, many of the threads generated by the off-diagonal nature of the forces involved in the momentum propagation steps are redundant. It is therefore desirable to selectively prune the large number of new threads created by the propagation procedure to retain only those threads which are necessary to represent the dynamical variable well. In recent publications,[11,12] we proposed various methods for maintaining a manageable number of total threads. The central idea in the ''multithreads'' algorithm is to combine threads which approach one another in classical phase space in a manner consistent with conservation principles. The utility of the combination principle relies on the notion that if two threads approach one another in a region in which the dynamical variable is smooth, one thread is likely to be redundant so that the two adjacent threads can be combined into a single thread. In the simplest implementation of the method, all nearest-thread pairs are searched for and then as many pairs of threads are combined as is necessary to keep the total number of threads at specific levels determined by issues such as the continuity of expectation values (such as populations or average trajectories) and energy conservation. Under these rules, the trajectories (threads) which are generated interact in a simple fashion, in contrast to most methods which use classical trajectories to describe quantum dynamics.

There are a number of critical issues to examine on a system-by-system basis to determine if the algorithm is practicable. Perhaps foremost among these is the number of threads necessary to describe the system and how this number scales with the number of classical degrees of freedom which are coupled to the quantum subsystem. In practice, it is often helpful to monitor the energy conservation to dynamically adjust the number of total threads as the system evolves. Similar kinds of ideas have been proposed by Martínez and co-workers[23] in the context of their ''multiple spawning'' method, in which a moving basis set with a dynamically adjusted size is used to solve the time-dependent Schrödinger equation. In classical molecular dynamics, dynamical evolution based on approximate propagators obtained from the Trotter expansion rigorously conserves[30,29] a pseudo-Hamiltonian which differs from the true Hamiltonian by a term of order Δt^3. Thus, provided Δt is small, the system evolves with no observed long-term drift in the energy in Verlet-style algorithms. In the multithreads algorithm, on the other hand, there is no corresponding pseudo-Liouville operator which ensures energy conservation due to the thread reduction procedure. However, each thread carries along an associated matrix (or supervector) whose elements measure the weight or importance of the thread to the overall average. Provided these weights are considered in the thread combination procedure such that, for instance, only a thread with small weight is allowed to combine with another thread, the net energy fluctuation caused by the thread combination can be limited. For systems in which the nonadiabatic coupling of two quantum states is relatively weak or highly localized in regions of classical configurational space, many of the threads which branch out of an original thread during a propagation step carry negligible weight. Combining these threads with others typically leads to very little energy drift. However, if the system has strong nonadiabatic coupling which extends over large regions of configurational space, many of the threads created by branching have significant weights so that combining them can lead to more serious problems with the conservation of energy and the continuity of observables. Under such circumstances one can anticipate that the total number of threads required by the method would be prohibitively large, particularly since much of the computational time involved in the method is spent in the routines searching for adjacent thread pairs. In spite of these concerns, the thread combination rules have been rigorously tested and have performed extremely well on several challenging one-dimensional systems in which complicated quantum interferences and tunneling are pronounced.[11,12]

One intriguing aspect of the method concerns the nature in which the initial discrete representation of the dynamical variables of interest is propagated. One extreme approach to

evaluating expectation values based on the trajectories would be to generate an initial number of initial number of threads L and then to propagate *each* initial thread independently (either sequentially or in parallel) starting from its initial value using the multithreads approach. Expectation values could then be calculated by averaging over the L runs. The opposite extreme would be to propagate all L initial threads *simultaneously* in one run while calculating expectation values on the fly. It is not clear which prescription, or hybrid variant of the two, is optimal as there are advantages and disadvantages to both approaches which must be counterbalanced. For example, if each L initial thread is propagated simultaneously, it is likely that a relatively large total number of threads is necessary to ensure energy conservation if the initial distribution from which the points are drawn is broad. On the other hand, only one run is necessary to extract the expectation values. In the other extreme, if each initial thread is propagated independently, then generally each run is well described by a modest number of maximum total threads, with the obvious drawback that many of these runs must be performed. In principle, the two approaches should give similar results. However, for systems in which the dispersion of the initial wave function is very important, significant differences between the two approaches could be observed. In fact, it seems likely that the optimal approach is sensitive to how ''classical'' the system is and is therefore highly system dependent. This aspect of the algorithm is currently being investigated.

Another concern that must be considered is the suitability of the multithreads method for multidimensional systems. In the multithreads approach, the effect of the multidimensional character of the system is intimately tied with the nature of the coupling of the classical degrees of freedom with the quantum subsystem. As is clear from the discussion above of the Trotter factorization, it is the fact that force matrices do not commute which gives rise to the additional branching of threads as the system evolves. The force matrices themselves, which govern the evolution of the phase space coordinates of the threads, are diagonal for any degrees of freedom which are not explicitly coupled to the quantum subsystem through the coupling potential $V_c(\hat{\mathbf{q}},\mathbf{R})$. The momentum propagation of these degrees of freedom does not lead to the branching of threads. Furthermore, the degrees of freedom which are explicitly coupled to the quantum subsystem may be grouped into classes in which the force matrices commute. For each force commutation class, the momentum degrees of freedom may be propagated together within the same representation so that the thread branching occurs only when switching between representations corresponding to different classes of degrees of freedom. Thus, the number of branching events per propagation time step is determined by the number of *classes* of noncommuting $i\mathcal{L}^P$. In many models which are used widely in the study of dynamics in condensed phases, such as the spin-boson model,[31] the form of the coupling between the quantum subsystem and each classical (spatial) degree of freedom is the same. For example, in the spin-boson model, the coupling is of a bilinear form $V_c=\gamma\hat{\mathbf{q}}R_i$, where γ is a parameter measuring the strength of the coupling, for all spatial coordinates R_i. For models with generic couplings of the form $V_c=\Sigma_i f(\hat{\mathbf{q}})g(R_i)$, all force matrices commute and all the momenta belong to the same force commutation class. For such models, only a single branching event occurs at each time step. However, other important models of chemical processes in condensed phases do not have a system–bath coupling which can be expressed in such a simple form. For instance, model studies of proton-transfer reactions in polar solvents generally involve a coupling between the proton motions,[32] which are described quantum-mechanically, and a *collective* solvent coordinate related to the solvent polarization.[33,34] For these systems, each momentum degree of freedom is potentially in a different force commutation class, and the manner in which the thread reduction is carried out is of critical importance. There are several different scenarios that are possible. If the thread reduction is done *after* all momentum propagation steps have been carried out for all the commutation classes, the number of threads that must be paired and combined will scale exponentially with the number of degrees of freedom. In this case, the multithreads method behaves as a grid method and is impracticable for large systems. It must therefore be demonstrated that the thread reduction procedure can be successfully conducted immediately after the momenta in each commutation class have been updated, leading to one thread reduction step for each class per time step. When this is possible, the multithreads method scales *linearly* with the number of force commutation classes and should be computationally feasible for large systems.

In the next section, we consider two simple multidimensional models for which the multithreads solution approach can be compared to exact quantum solutions. The models differ in the number of commutation classes so that the scaling behavior of the multithreads algorithm can be assessed.

IV. TWO-DIMENSIONAL MODEL SYSTEMS

The multithreads method was tested on model two-dimensional systems designed to describe important physical processes in which the multidimensional nature of the coupling of quantum subsystem (electronic degrees of freedom) to motions of heavy particles (nuclei) induces complicated quantum dynamics. The models differ qualitatively in the nature of the coupling and therefore together pose a significant test of the multithreads method. In all calculations below, the basic rules of thread combination of Ref. 12 were followed: Namely, the weight matrix (or supervector) $\mathbf{W}$ for a new thread formed by the combination of two adjacent threads was taken to be $\mathbf{W}=\mathbf{W}_1+\mathbf{W}_2$, where $\mathbf{W}_1$ and $\mathbf{W}_2$ are the (complex) ''weight'' factors for the two combining threads, whereas the phase space coordinate $\mathbf{X}=(\mathbf{R},\mathbf{P})$ for the new thread was determined by $\mathrm{Tr}\,\mathbf{W}\mathbf{X}=\mathrm{Tr}\,\mathbf{W}_1\mathbf{X}_1+\mathrm{Tr}\,\mathbf{W}_2\mathbf{X}_2$, where $\mathbf{X}_1$ and $\mathbf{X}_2$ are the respective phase space coordinates for the combining threads. The expectation values themselves were formed by averaging over roughly ten runs of a relatively modest number of threads (around 300 maximum threads). In each run, the initial number of threads was kept constant and the time step was set by requiring energy conservation of roughly 1% over the entire run. All runs were based upon a diabatic reference basis for the quan-

tum subsystem. In the diabatic reference basis, the quantum rotation part of the Liouvillian $i\mathcal{L}^Q$ [see Eq. (10)] is particularly simple to evaluate since the basis set is independent of $\mathbf{R}$ and the nonadiabatic coupling matrix $\mathbf{D}$ is zero. In all the tests below, the results of the multithreads algorithm are compared to the exact (numerical) quantum dynamics of the models. The full dynamics was carried out using fast Fourier transform methods (FFT) based on a two-dimensional grid of roughly 500×500 points. In the cases considered below, the initial wave packet was taken to be a product of Gaussian wave packets on a specific diabatic surface and originally positioned in an asymptotic region well removed from regions of appreciable population transfer.

A. Collinear reactive collision model

The first two-dimensional test considered is a model of the collinear reaction of three atoms of the form $A+BC \rightarrow AB+C$ utilized by Ben-Nun and Martínez to validate the multiple spawning molecular dynamics method.[23] The Hamiltonian is constructed by coupling two diabatic states 1 and 2, each of which describes a collinear nonreactive collision between an atom and a diatomic molecule: $A+BC$ on the first diabatic surface, and $AB+C$ on the other. Each of the diabatics is given by a sum of two terms: a Morse oscillator describing the AB or BC vibration and an exponentially repulsive functional form for the interaction of the bound species with the third atom:[23]

$$V_{1,1}(r,R)=D_e(1-e^{-\beta(r-r_e)})^2 + D_{\mathrm{rep}}e^{-\beta(R-0.5r-r_e)},$$
$$V_{2,2}(r,R)=D_e(1-e^{-\beta(R-0.5r-r_e)})^2 + D_{\mathrm{rep}}e^{-\beta(r-r_e)}, \quad (36)$$

where r is the distance between atoms B and C; R is the distance from atom A to the center of mass of the diatomic BC. The parameters appearing in (36) were taken to be $D_e=0.038\,647$, $\beta=0.458\,038$, $r_e=5.0494$, and $D_{\mathrm{rep}}=0.02$ in atomic units. The partially Wigner-transformed Hamiltonian of the system for this model can be written as

$$\hat{H}_w(r,p,R,P)=\frac{p^2}{2m}+\frac{P^2}{2M}+\mathbf{V}(r,R)+\mathbf{V}_c, \quad (37)$$

where $\mathbf{V}(r,R)$ is the (diagonal) diabatic matrix in (36), and p and P are the classical momenta conjugate to the r and R coordinates, respectively. In Eq. (37), $\mathbf{V}_c$ is a constant, off-diagonal 2×2 matrix with diagonal elements of zero and off-diagonal elements $V_c=0.001\,36$ in atomic units. The masses $m=M_{\mathrm{Li}}/2$ and $M=2M_{\mathrm{Li}}/3$ were taken to correspond to the reduced masses for the BC and the $A-BC$ motions when atoms A, B, and C are lithium.

The resulting ground-state adiabatic potential energy surface describes a reactive atom exchange with a barrier height of 0.435 36 eV and is qualitatively of the London–Eyring–Polanyi–Sato form.[35] The excited-state adiabatic potential energy surface describes a bound linear triatomic molecule Li_3^*. At the saddle point of the ground-state adiabatic surface, the two adiabatic surfaces are separated by $2V_c=0.002\,72$ a.u. ($600\ \mathrm{cm}^{-1}$).[23] Note that in this model, since the potential energy surfaces are anharmonic and the r and R coordinates are strongly coupled, the potentials are nonseparable in r and R and hence are not quasi-one-dimensional. Furthermore, the two adiabatic surfaces are very dissimilar, which suggests that mean-field dynamical prescriptions will break down.[36]

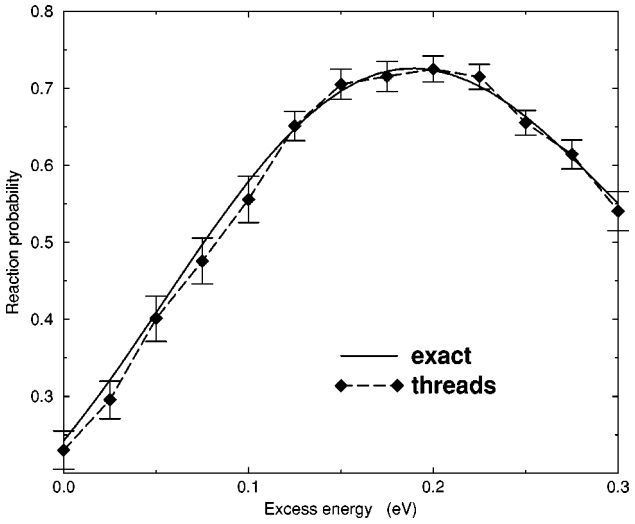

FIG. 1. The diabatic reaction probability as a function of the excess energy in eV for the collinear reactive collision model. The full line represents the numerical solution of the model, and the dashed line the averaged (over ten runs) multithreads solution of the mixed quantum-classical Liouville equation. The multithreads runs all started from an initial number of 300 threads, randomly drawn from the initial distribution, and the number of threads was held at all times to the initial number through the pruning/combination rules described in the text.

As mentioned above, all calculations were carried out in the diabatic representation. The initial state of the system for all runs reported below was specified by an initial nuclear wave function taken to be a product of two one-dimensional Gaussians centered in the asymptotic region in which the atom is separated from the center of mass of the diatomic by 16 bohr (i.e., $R=16$ bohr). The width of the Gaussians for both r and R was taken to be 2 bohr^{-1}. Only the first diabatic state in which the BC atoms are bound was initially populated and the diatomic was in the ground vibrational state. For the multithreads runs, the initial classical phase space coordinates were drawn from the corresponding Wigner transform of the density matrix for the conditions described above. Following Ref. 23, a broad range of relative kinetic energies, $P^2/2M$, for the atom with respect to the diatomic was studied. The relative kinetic energy was classified in terms of the excess energy, defined to be the difference between the relative kinetic energy and the reactive barrier height on the ground-state adiabatic energy surface (0.435 36 eV). The excess energy values ranged from 0.0 eV, where quantal effects such as above the barrier reflection and tunneling are prominent, to a value of 0.3 eV, where population may be trapped in the excited-state well and slowly leak out via nonadiabatic effects.

In Fig. 1, the diabatic reaction probability as a function of the excess energy is plotted for the full quantum solution and the multithreads method. Note that the multithreads results agree with the full quantum results within the statistical

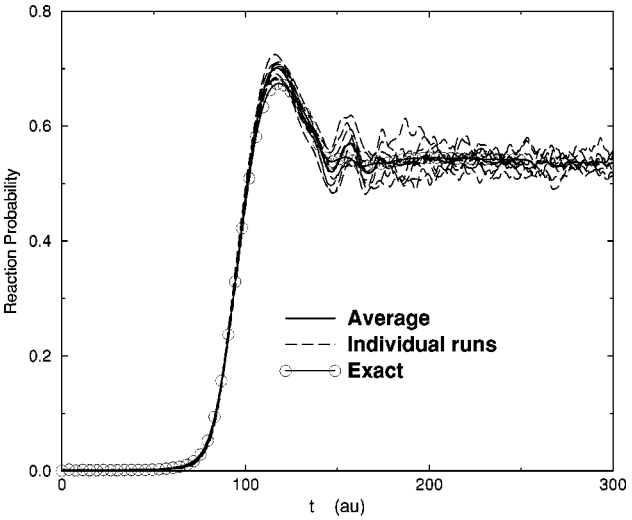

FIG. 2. The diabatic reaction probability as a function of time at an initial excess energy of 0.3 eV for the collinear reactive collision model. The solid line with and without circles represents numerical solution of the model and the averaged multithreads solution, respectively, and the dashed lines indicate the time profile of individual runs.

uncertainties associated with averaging over ten propagation runs starting from an initial multithread basis of 300 threads. In each of the runs, the maximum number of threads was kept fixed at 300 threads and the time step of propagation, determined by requiring energy conservation of all runs at all times to within 1%, was 0.1 atomic units. Each run took roughly 5 min. on a modern workstation (DEC alpha, 500 MHz, 21164 processor). In all runs, the expectation values of r and R as well as the branching ratios were monitored to determine when the system reached the asymptotic region. The reaction probability was then interpreted as the population of the second diabatic state after the system stabilized. In Fig. 2 the spread in the diabatic reaction probability as a function of time is shown from the ten runs at an excess energy of 0.3 eV. The spread in the diabatic reaction probability for runs at other values of the excess energy was comparable to that shown in Fig. 2. Note that the spread in the data increases markedly at times of roughly 100 atomic units where the evolving density matrix enters the reactive region of the adiabatic potential energy surface.

For the particular form of the interaction between diabatic surfaces

$$\frac{\partial V_c}{\partial r}=\frac{\partial V_c}{\partial R}=0, \tag{38}$$

which implies that the force matrices are diagonal in the diabatic basis and therefore commute. Both p and P are therefore in the same force commutation class and hence $i\mathcal{L}^p$ and $i\mathcal{L}^P$ can be simultaneously diagonalized. For the collinear reactive collision model with a constant coupling matrix $\mathbf{V}_c$, only one thread-branching event occurs per time step. As a simple test of the multidimensional version of the thread propagation combination rules, additional runs were carried out in which the threads were sequentially propagated along each classical phase space "direction" (r,p) and (R,P) according to the Trotter decomposition in Eq. (20). The thread combination (reduction) step was carried out after each momentum propagation as though the propagators iLo^p and $i\mathcal{L}^P$ were in different commutation classes. Even though the thread combination was conducted more frequently, leading to a factor of 2 increase in the total computational time of the runs, no significant difference in the results for the reaction probability or other observables was observed. Furthermore, in order to examine the sensitivity of the runs on the basis set used to represent the quantum operators, the runs were repeated with an adiabatic basis reference set. Although in principle the propagation schemes depend on the reference basis set through the representation of the time propagator $i\mathcal{L}$ and the weights used in the combination of threads, no statistically significant differences were noted from the results obtained in the diabatic reference basis.

B. Conical intersection model

Although the previous model provides a rigorous test of some features of the multithreads method applied to anharmonic, multidimensional systems with nonseparable Hamiltonians and avoided crossings, the simple form of the coupling matrix leads to a single force commutation class. We now turn our attention to a two-dimensional model of conical intersections proposed several years ago by Ferretti *et al.*[24] in which the qualitative nature of the quantum dynamics *and* the spatial dependence of the nonadiabatic coupling are substantially different from the collinear reactive collision model. The conical intersection model[24,37] was designed to study the dynamics of a wave packet crossing a conical intersection modeled by two-dimensional diabatic potentials. The dynamics consists of a wave packet, initially in the first excited adiabatic state, propagating along a low-frequency coordinate X while oscillating around the other coordinate Y in the two-dimensional system. As in Ref. 24, we limit our study to a single passage of the wave packet through the strong interaction region in the vicinity of the conical intersection. The dynamics may therefore be appropriate for photodissociative processes or strongly dissipative processes in which no recurrences are observed.

The Hamiltonian for the conical intersection model can be written in a diabatic representation in terms of symmetric and antisymmetric stretch coordinates X and Y of a linear triatomic molecule ABA as[24]

$$\begin{aligned} H_{11}(X,Y)&=\frac{K_x}{2}(X-X_1)^2+\frac{K_y}{2}Y^2,\\ H_{22}(X,Y)&=\frac{K_x}{2}(X-X_2)^2+\frac{K_y}{2}Y^2+\Delta,\\ H_{12}(X,Y)&=H_{21}(X,Y)=\gamma Y e^{-\alpha(X-X_3)^2}e^{-\beta Y^2}. \end{aligned} \tag{39}$$

The parameters appearing in Eq. (39) are, in atomic units,

$$\begin{aligned} &K_x=0.02, \quad K_y=0.10, \quad \Delta=0.01,\\ &X_1=4, \quad X_2=3, \quad X_3=3,\\ &M_x=20\,000.0, \quad M_y=6667.0,\\ &\alpha=3.0, \quad \beta=1.5. \end{aligned} \tag{40}$$

The parameter γ measuring the coupling between the diabatic surfaces was varied from values characterizing the weak-coupling regime ($\gamma=0.005$ a.u.) to the strong-coupling regime ($\gamma=0.08$ au). For small coupling strengths, the ground adiabatic surface has a single minimum at $X\approx 4$, $Y=0$ while for larger γ two minima appear at smaller X with opposite values of Y (see Ref. 36 for a more detailed description of the potential energy surfaces in the model). Due to the X dependence of the coupling between the diabatic H_{11} and H_{22} surfaces, the nonadiabatic region in which most of the population transfer occurs is in the region of $X\approx 3$.

For this model, we focus on the probability of the ground adiabatic state after a single passage through the strong coupling region as a function of the coupling strength γ. Following Ref. 24, the initial state for the full quantum simulations was taken to be a Gaussian wave packet on the first *diabatic* state ψ_1 of the form

$$\psi_1(X,Y)\approx\chi_2(X,Y) = (\pi\Delta X\Delta Y)^{-1/2}e^{-(X-X_0)^2/2\Delta X^2}e^{-(Y-Y_0)^2/2\Delta Y^2}, \tag{41}$$

where χ_2 is the wave function for the excited adiabatic state and the widths are $\Delta X=0.150$ and $\Delta Y=0.197$ bohr. These initial conditions were chosen to mimic a Franck–Condon excitation to the first excited state from a ground state coupled to the adiabatic states through an infinitely short radiation pulse.[24] The center of the wave packet is at $X_0=2.0$, $Y_0=0.0$, which corresponds to a region where the nonadiabatic coupling is small and the first excited adiabatic state χ_2 is approximately given by the first diabatic wave function ψ_1. The initial thread positions in the classical phase space (X,Y,P_x,P_y), where P_x and P_y are the momenta conjugate to X, and Y, were drawn from the (partial) Wigner transform of Eq. (41).

In the diabatic basis, the Liouville superoperator has off-diagonal elements in both the quantum rotation part $i\mathcal{L}^Q$ and in the momentum propagation part of both P_x and P_y. Due to the nonsymmetric functional dependence on X and Y of the nonadiabatic coupling term $H_{12}(X,Y)$, the force operators F_x and F_y do *not* commute. Hence, the conical intersection model provides a nontrivial test of the multithreads method for systems in which more than one force commutation class exists and multiple thread branching and reduction events occur per time step.

The results of the exact quantum calculation and the multithreads calculation of the populations of the ground adiabatic state as a function of the nonadiabatic coupling strength after a single passage through the strong coupling region are shown in Fig. 3. The adiabatic populations shown were obtained by allowing the system to propagate through the strong coupling region and waiting for the adiabatic populations to stabilize. For all coupling strengths, the stabilization time was roughly 50 a.u. The multithreads populations for the weak coupling limit ($\gamma\leqslant 0.04$) were calculated based on ten runs in which 328 initial threads were propagated with a time step of about 0.02 a.u. However, when the nonadiabatic coupling strength γ was larger than 0.04, the populations of the adiabatic states developed discontinuities

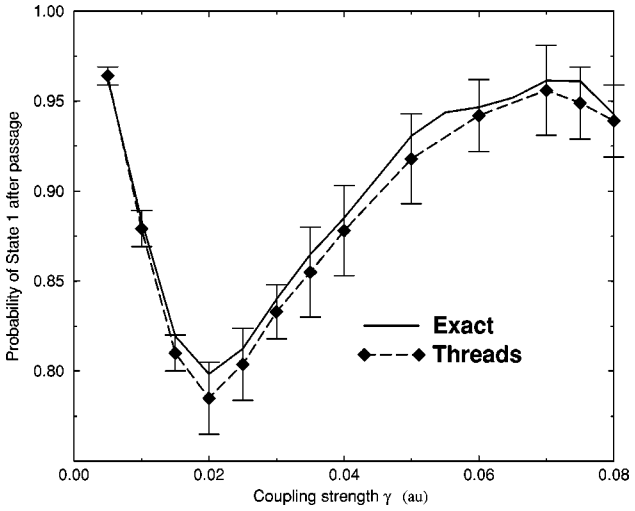

FIG. 3. The population of the ground adiabatic state as a function of coupling strength γ after the first passage through the nonadiabatic coupling region for the conical intersection model. The solid lines are the exact numerical solution of the model, and the diamonds connected by the dashed line are the result obtained from the multithreads approach.

signaling a failure in the thread reduction procedure. Enlarging the initial number of threads to 512 threads was still not sufficient to smooth out the discontinuities for the runs with larger nonadiabatic coupling. In principle, one could improve the continuity of the data by allowing for an even larger maximum number of threads, but expanding the set of threads drastically increases the time required for each run. As an alternative, the way in which the initial number of threads was sampled from the distribution was modified based on the observation that, although the adiabatic populations as a function of time vary for different initial values of P_x, the asymptotic value of the populations after passage through the region of strong coupling is relatively insensitive to the initial value of P_x. The asymptotic value of the adiabatic populations calculated over the runs therefore converges relatively quickly if the initial threads are a chosen to have the same initial value of P_x (randomly selected from the distribution) while the other degrees of freedom are sampled without restriction. However, since the spread in the populations at intermediate times for runs with different initial P_x is much greater than that in the asymptotic regions, a larger number of runs would be required to reproduce the profile of the adiabatic populations at a given level of statistical uncertainty when γ is large. This behavior is evident in Fig. 4, in which the population of the ground adiabatic state is plotted as a function of time for $\gamma=0.01$ and $\gamma=0.08$, corresponding to the weak and strong coupling regimes. One may speculate that the failure of the multithreads in the strong coupling regime when the initial thread points are sampled uniformly from the initial distribution arises from the fact that the dispersion in the distribution along the P_x dimension implies that some threads move with quite different velocities along the X direction of the potential energy surface. As a consequence, individual threads move through the nonadiabatic region near $X=3.0$ at different times so that the strong branching events do not interact with one another, leading to discontinuous changes in population when threads

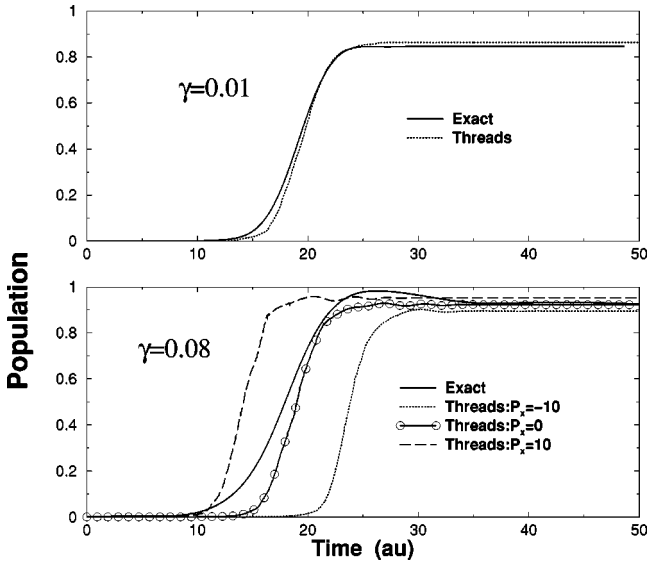

FIG. 4. The adiabatic population as a function of time for the conical intersection model. In the two panels, the exact numerical solution (solid line) and the multithreads solution (dotted line) are plotted as a function of time for the case of weak coupling (upper panel, $\gamma=0.01$), and strong coupling (lower panel, $\gamma=0.08$).

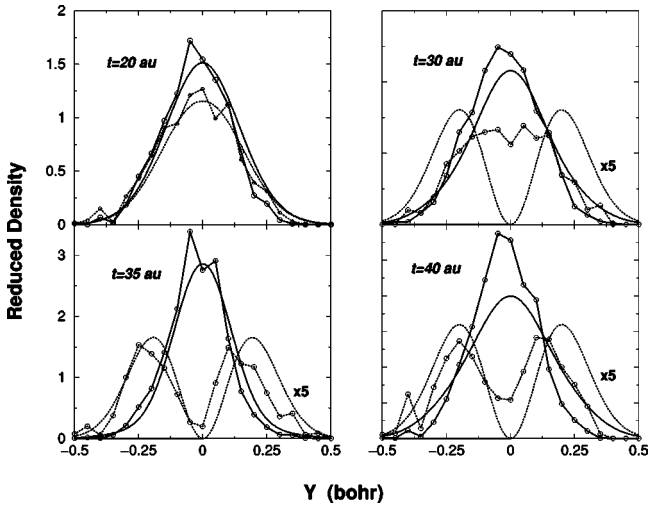

FIG. 5. The reduced densities $\rho^{(q)}(Y,t)$ and $\rho^{(cl)}(Y,t)$ as a function of Y at different times (in atomic units) for the weak-coupling case ($\gamma=0.01$).

are combined. These discontinuities are not reflected in the norm, which is conserved by the thread combination procedure. In all the runs used to calculate the populations shown in Fig. 3, the total number of threads at all time steps was kept equal to the number of initial threads by the thread reduction procedure and the energy was conserved to within 4%. The runs with 328 initial threads took roughly 3 min on a 933 MHz Pentium III processor, while the runs for stronger coupling took around 8 min. As is clear from Fig. 3, the ground-state adiabatic population calculated using the multithreads approach agrees extremely well for all coupling strengths in contrast to a surface-hopping approach[4] where the populations differ by 10%–20% from the exact result for coupling strengths $\gamma \geqslant 0.02$.[24]

Although branching ratios and reaction probabilities are important observables, they are often somewhat insensitive to subtle features of the quantum system and tend to wash out fine structural detail which is evident in the density matrix. It is therefore interesting to examine directly the fine structure of reduced densities of the full density matrix[38]

$$\rho_{11}^{(q)}(Y,t)=\int dX\,\rho_{11}(X,Y,t),$$

$$\rho_{22}^{(q)}(Y,t)=\int dX\rho_{22}(X,Y,t), \tag{42}$$

with their mixed quantum-classical analogs

$$\rho_{11}^{(cl)}(Y,t)=\int dX\,dP_x\,dP_y\,\rho_w^{11}(X,Y,P_x,P_y,t),$$

$$\rho_{22}^{(cl)}(Y,t)=\int dX\,dP_x\,dP_y\,\rho_w^{22}(X,Y,P_x,P_y,t). \tag{43}$$

In Fig. 5 the reduced densities $\rho^{(q)}$ and $\rho^{(cl)}$ as a function of Y are shown at different times for $\gamma=0.01$. The reduced classical densities $\rho^{(cl)}(Y,t)$ were obtained from a single run of 1000 initial threads drawn without restriction from the initial distribution. They were estimated via weighted histograms formed by summing the targeted matrix element (either 1,1 or 2,2) of all matrices within a given range of Y and then normalized according to $\mathrm{Tr}\int dY\,\rho^{(cl)}(Y,t)=1$. As described by Ferretti *et al.*,[24] the wave packet does not spread appreciably or decrease in magnitude on the first excited adiabatic state in the Y direction until it reaches the nonadiabatic region at times near $t=20$ a.u. at which point there is a rapid transfer of population into the ground state. The population transfer corresponds to a splitting of the wave packet into a small component that remains on the excited state and a larger component that subsequently propagates forward on the ground state. After passing through the strong-coupling region, the component of the wave packet that remains in the excited state develops a node at $Y=0$ which persists through to the asymptotic region. As noted by Ferretti *et al.*,[24] the appearance of the node is a manifestation of Berry's phase. Similar features have been observed in the study of wave packet dynamics of Na_3.[39]

It is interesting to note that although there is a hint of a node appearing in $\rho_{22}^{(cl)}(Y,t)$ at some times, the node disappears and reappears as the system evolves beyond the region of strong coupling. The underlying reason for this behavior is not clear and may arise from the approximate nature of the mixed quantum-classical Liouville equation or from the choice of poor thread reduction rules. It should be emphasized that the dynamical evolution scheme outlined here is only approximate and may no longer be valid when the quantum behavior of the coordinates which are treated ''classically'' becomes important. Further work examining when the mixed quantum-classical description breaks down is clearly necessary.

One may also examine reduced densities along the X coordinate. These plots, however, do not show the rich behavior observed in $\rho^{(q)}(Y,t)$ and are fairly well reproduced

by the multithreads method as well as by other semiclassical methods.[24] One can also examine the reduced densities at higher coupling strengths. At higher coupling, the number of nodes that appear in $\rho_{22}^{(q)}(Y,t)$ after passing through the strong-coupling region increases and much finer structure appears in the reduced density. These features are also qualitatively reproduced in $\rho^{(cl)}(Y,t)$, although the detailed structure tends to be only approximately correct. It is interesting that as the coupling strength increases, the structural features in the reduced density $\rho^{(q)}(Y,t)$ become increasingly sharp. As the multithreads algorithm relies on the smoothness of the quantities such as the partial Wigner transform of the density matrix $\rho_w(\mathbf{R},\mathbf{P},t)$, it is not surprising that more and more threads are required as the strong-coupling limit is approached if quantitatively accurate results are desired.

V. SUMMARY

In this article, the multithreads algorithm[11,12] was extended to multidimensional systems and tested on simple two-dimensional models for which the exact quantum solution is readily attainable. The scheme is based on a Trotter decomposition of the mixed quantum-classical Liouville equation in which noncommuting force operators represented as off-diagonal matrices or supervectors in the quantum representation lead to trajectory branching at each time step. It is demonstrated that the number of branching events per time step is determined by the number of force commutation classes for the system.

In order to determine how the method scales with the dimensionality and number of commutation classes in the system, the multithreads algorithm was tested on two models designed to probe different aspects of the method. The first model considered was the two-dimensional collinear reactive collision model of Martínez and co-workers.[23] Unlike many other benchmark tests designed to compare approximate methods of nonadiabatic molecular dynamics with exact numerical results, the dynamics of the two coordinates is governed by a nonseparable Hamiltonian at all times. Furthermore, the form of the diabatic potentials and the coupling lead to ground and excited adiabatic potential energy surfaces which differ qualitatively; the ground-state surface describes a reactive collision while the excited-state surface describes a bound triatomic complex. In spite of these aspects of the model, which make it a stringent test of semiclassical approaches, the multithread algorithm yields results which show excellent agreement for the diabatic reaction probability with the exact numerical solution of the model when as few as 300 threads initially sampled from a Gaussian distribution are propagated. In addition, the time profile of the diabatic reaction probability is reproduced quite well. The quality of the results obtained is insensitive to the way in which the propagation is carried out, namely whether the thread reduction procedure is done after the propagation of each momentum coordinate or not, as well as to the choice of reference basis for the quantum subsystem.

Unfortunately, the simple form of the coupling term in the collinear reactive collision model leads to a single force commutation class. To examine how the multithreads approach works for multidimensional systems with diabatic coupling terms which depend explicitly on the classical coordinates, a two-dimensional model of a conical intersection was considered. In the conical intersection model, the particular form and functional dependence of the diabatic coupling term implies that the two force operators which appear in the momentum propagator do not commute. For this model, the multithreads algorithm was applied by carrying out the thread reduction step after each momentum degree of freedom was propagated, and excellent agreement between the resulting adiabatic populations and the exact populations after first passage through the strong-coupling region was obtained in the weak-coupling regime using roughly 300 threads. In the strong-coupling limit, however, when uniform sampling of the classical phase space coordinates of the initial threads was utilized, discontinuous changes in populations and expectation values of coordinates were observed. This problem was remedied by changing the sampling scheme used to select the initial coordinates of the threads based on the observation that the dispersion in P_x in the initial distribution had relatively little effect on the asymptotic value of the adiabatic populations. When the same initial values of P_x randomly chosen from the initial distribution were used for all 512 threads, relatively few runs were needed to obtain the correct asymptotic populations within statistical uncertainties of roughly 5%. Reduced densities for the coordinate Y were also considered for the conical intersection model and it was demonstrated that although many of the qualitative features observed in the quantum reduced densities $\rho^{(q)}(Y,t)$ were reproduced in the classical reduced densities $\rho^{(cl)}(Y,t)$, important differences appeared in the nodal structure of the reduced densities for the system in the excited adiabatic state after passage through the strong-coupling region. The nodal structure are a manifestation of Berry's geometrical phase,[22] and perhaps are not correctly reproduced due to the approximate nature of the mixed quantum-classical description in which the evolution of the X and Y coordinates is treated in ''classical'' fashion.

A number of important issues concerning the method outlined in this paper remain to be examined. Perhaps foremost among these is the range of validity of the multithreads algorithm so that one may gain some understanding as to what specific conditions must be met for such an approach to be fruitful. In particular, understanding how the thread rules influence energy conservation and how the (chaotic) nature of the classical trajectories relates to the smoothness of the density matrix is fundamental to obtaining a clearer picture of the utility of the algorithm. Unfortunately, the ''uncontrolled'' nature of the thread reduction procedure make direct theoretical investigation of such concerns difficult, and it is clearly desirable to develop a sound theoretical framework to examine the method for simple systems. Efforts along these directions are underway.

ACKNOWLEDGMENTS

The authors would like to thank T. Martínez for useful discussions about the collinear reactive collision model. This work was supported by a grant from the Natural Sciences and Engineering Research Council of Canada.

[1] R. Kapral and G. Ciccotti, J. Chem. Phys. **110**, 8919 (1999).
[2] V. S. Filinov, S. Bonella, Y. L. Lozovik, A. V. Filinov, and I. Zacharov, ''Quantum molecular dynamics using Wigner representation,'' in *Classical and Quantum Dynamics in Condensed Phase Simulations*, edited by B. J. Berne, G. Ciccotti, and D. Coker (World Scientific, Singapore, 1998).
[3] O. V. Prezhdo and P. J. Rossky, J. Chem. Phys. **107**, 825 (1997).
[4] J. C. Tully, J. Chem. Phys. **93**, 1061 (1990); Int. J. Quantum Chem. **25**, 299 (1991); S. Hammes-Schiffer and J. C. Tully, J. Chem. Phys. **101**, 4657 (1994).
[5] J. C. Tully, Int. J. Quantum Chem. **25**, 299 (1991); S. Hammes-Schiffer and J. C. Tully, J. Chem. Phys. **101**, 4657 (1994).
[6] F. Webster, P. J. Rossky, and R. A. Friesner, Comput. Phys. Commun. **63**, 494 (1991); F. J. Webster, J. Schnitker, M. S. Friedrichs, R. A. Friesner, and P. J. Rossky, Phys. Rev. Lett. **66**, 3172 (1991).
[7] D. F. Coker and L. Xiao, J. Chem. Phys. **102**, 496 (1995).
[8] X. Sun and W. H. Miller, J. Chem. Phys. **106**, 916 (1997); **106**, 6346 (1997).
[9] A. Donoso and C. C. Martens, J. Phys. Chem. **102**, 4291 (1998); A. Donoso, D. Kohen, and C. C. Martens, J. Chem. Phys. **112**, 3980 (2000); A. Donoso and C. C. Martens, *ibid.* **112**, 7345 (2000).
[10] G. Stock and M. Thoss, Phys. Rev. Lett. **78**, 578 (1997).
[11] C.-C. Wan and J. Schofield, J. Chem. Phys. **112**, 4447 (2000).
[12] C.-C. Wan and J. Schofield, J. Chem. Phys. **113**, 7047 (2000).
[13] For a review of quasiclassical trajectory methods, see *Advances in Classical Trajectory Methods*, edited by W. L. Hase (Jai, London, 1992), Vol. 1.
[14] W. H. Miller, J. Chem. Phys. **95**, 9428 (1991); E. J. Heller, *ibid.* **94**, 2723 (1991); **95**, 9431 (1991); G. Stock and M. Thoss, Phys. Rev. Lett. **78**, 578 (1997); M. F. Herman and E. Kluk, Chem. Phys. **91**, 27 (1984); K. G. Kay, J. Chem. Phys. **100**, 4377 (1994); **100**, 4432 (1994).
[15] X. Sun, H. Wang, and W. H. Miller, J. Chem. Phys. **109**, 7064 (1998).
[16] W. Boucher and J. Traschen, Phys. Rev. D **37**, 3522 (1988).
[17] O. V. Prezhdo and V. V. Kisil, Phys. Rev. A **56**, 162 (1997).
[18] C. C. Martens and J.-Y. Fang, J. Chem. Phys. **106**, 4918 (1997).
[19] T. J. Martínez and R. D. Levine, J. Chem. Soc., Faraday Trans. **93**, 940 (1997); T. J. Martínez, M. Ben-Nun, and R. D. Levine, J. Phys. Chem. **101**, 6389 (1997).
[20] J.-Y. Fang and S. Hammes-Schiffer, J. Chem. Phys. **107**, 8933 (1997).
[21] H. C. Longuet-Higgins, Proc. R. Soc. London, Ser. A **344**, 147 (1975).
[22] M. V. Berry, Proc. R. Soc. London, Ser. A **392**, 45 (1984).
[23] M. Ben-Nun and T. J. Martínez, J. Chem. Phys. **108**, 7244 (1998).
[24] A. Ferretti, G. Granucci, A. Lami, M. Persico, and G. Villani, J. Chem. Phys. **104**, 5517 (1996).
[25] E. Wigner, Phys. Rev. **40**, 749 (1932).
[26] For the Trotter formula to apply in Hilbert space, the spectrum of all linear operators to which the factorization is applied must be purely imaginary for time-reversible dynamics. For a discussion of the Trotter product formula applied to physics, see E. Nelson, J. Math. Phys. **5**, 332 (1964).
[27] W. C. Swope, H. C. Andersen, P. H. Berens, and K. R. Wilson, J. Chem. Phys. **76**, 637 (1982).
[28] G. D. Quinlan and S. Tremaine, Mon. Not. R. Astron. Soc. **259**, 505 (1992).
[29] S. Toxvaerd, Phys. Rev. E **50**, 2271 (1994).
[30] H. Yoshida, ''Simplectic integrators for Hamiltonian systems: Basic theory,'' in *Chaos, Resonance and Collective Dynamical Phenomena in the Solar System*, edited by S. Ferrz-Mello (Kluwer, Dordrecht, 1992), pp. 407–411.
[31] A. J. Leggett, S. Charkavarty, A. T. Dorsey, M. P. A. Fisher, A. Garg, and W. Zwerger, Rev. Mod. Phys. **59**, 1 (1987).
[32] D. Laria, G. Ciccotti, M. Ferrario, and R. Kapral, Chem. Phys. **180**, 181 (1994).
[33] A. Warshel, J. Am. Chem. Soc. **86**, 2218 (1982).
[34] R. A. Marcus and N. Sutin, Biochim. Biophys. Acta **811**, 265 (1985).
[35] R. D. Levine and B. R. Bernstein, *Molecular Reaction Dynamics and Chemical Reactivity* (Oxford University Press, New York, 1987).
[36] G. D. Billing, Int. Rev. Phys. Chem. **13**, 309 (1994).
[37] A. Ferretti, A. Lami, and G. Villani, J. Chem. Phys. **107**, 3498 (1997).
[38] R. Schneider, W. Domcke, and H. Köppel, J. Chem. Phys. **92**, 1045 (1990).
[39] J. Schön and H. Köppel, Chem. Phys. Lett. **231**, 55 (1994).